Int. J. Nanosci. Nanotechnol., Vol. 20, No. 2, June 2024, pp. 129-142
DOI: 10.22034/ijnn.2024.2022011.2474

Lithium Extraction by Metal Organic Framework-Based Adsorbent (MnO_2@Co/Zn ZIF) from Aqueous Solutions

Saman Mesvari[1], Mojtaba Shariaty-Niassar[1,*], Javad Karimi-Sabet[2] and Abolfazl Dastbaz[2]

[1]Department of Chemical Engineering, Faculty of Engineering, University of Tehran, Tehran, Iran
[2]Material and Nuclear Fuel Research School (MNFRS), Nuclear Science and Technology Research Institute, Tehran, Iran

(*) Corresponding author: mshariat@ut.ac.ir
(Received: 03 February 2024 and Accepted: 18 May 2024)

Abstract

Lithium is one of the critical elements in the development of industries, and its amount in seawater and brines (2.5×10^{11} tonnes) is estimated to be about 16,000 times more than land-based resources. However, the low lithium concentration in seawater (0.17 ppm) requires an efficient and selective method of lithium extraction. Although metal-organic frameworks (MOFs) are widely utilized for removing or extracting heavy metals from seawater, they have not been extensively employed for lithium extraction from such sources. This research used a bimetallic MOF-based adsorbent (MnO_2@Co/Zn ZIF) to extract lithium ions from the solution. The effects of Li^+ concentration and contact time on adsorption were investigated. Based on kinetic studies, the pseudo-second-order model adequately represents the kinetic behavior of lithium adsorption. The thermodynamic study demonstrated lithium adsorption with MnO_2@Co/Zn ZIF is endothermic, spontaneous, and physisorption. The adsorption process fitted well with the Freundlich isotherm (R^2=0.994), and this isotherm showed the maximum adsorption capacity at room temperature to be 71.43 mg/g. The desorption process was carried out with an HCl solution and showed that MnO_2@Co/Zn ZIF has excellent desorption ability. In addition, it was demonstrated that the adsorbent could be used for lithium adsorption after three cycles of regeneration. Moreover, MnO_2@Co/Zn ZIF is a viable candidate for recovering large amounts of lithium ions from solutions, based on the results.

Keywords: *Lithium, Adsorption, Separation, Metal-Organic frameworks, MOFs.*

1. INTRODUCTION

Recently, Lithium has been frequently used in various industries, such as rechargeable batteries, special glasses and glass ceramics used in dentistry, air conditioning, and industrial drying systems, drugs to treat manic depression, storing hydrogen for use as a fuel, reducing corrosion and erosion rates, reducing melting point and viscosity, general-purpose lubricating grease, organic and polymer chemistry, light alloys and the production of deuterium and tritium as fuel for nuclear fusion. Therefore, the increase in demand for lithium can be related to the development of these industries [1].

Despite the low concentration of lithium (about 17 mg. L^{-1}), the ocean contains about 230 billion tons of lithium, four orders of magnitude larger than the lithium reserves on land [2]. Several methods, such as adsorption, solvent extraction, and co-precipitation, have been studied to extract lithium from brine, seawater, and geothermal water. Compared to other methods, adsorption offers many advantages, such as simplicity, low operating costs, low energy consumption, high lithium uptake capacity, environmental friendliness, and superior lithium selectivity [3]. Therefore,

adsorption is a highly effective for recovering and extracting lithium from seawater.

Common adsorbents for lithium adsorption include ion sieves (such as LMO and LTO) [4, 5], polymer composites containing crown ether groups [6, 7], zeolites [8], activated carbon [9], and natural adsorbents such as roasted date pits [10].

Metal-organic frameworks (MOFs) are a type of adsorbent material that consist of organic and inorganic components. They are crystalline and porous in structure, with a regular and repeating arrangement of metal ions surrounded by organic molecules that act as connecting links or linkers. The combination of the metal centers and organic linkers creates a highly porous and customizable material that can be used for adsorption applications [11]. Since MOFs are porous and have high surface areas, they can be used in various applications, including adsorption, drug delivery, separations, storage, catalysis, and sensors [12, 13].

MOFs can be used to adsorb/extract metals from different matrices, including water. In this regard, MOF-based adsorbents have been used to adsorb metal ions such as Pb, Pd, Hg, Cu, Cd, Th, U, Ni, Cr, Zn, Mn, and Co [14-28]. However, there is limited research on the adsorption of alkaline and alkaline earth metal ions, such as Li+, by metal-organic framework (MOF) structures.

In 2018, Huacheng Zhang et al. reported that alkali metal ions could be transported ultrafast in MOF-based membranes, such as ZIF-8 or UiO-66 membranes. These structures have uniform sub-nanometer pores, consisting of angstrom-sized windows and nanometer-sized cavities. Also, alkali metal ions were selected by angstrom-sized windows, whereas ultrafast ions were transported by nanometer-scale cavities [29]. In 2019, Sang Ho Park et al. developed biomimetic phosphonate metal-organic framework (pMOF)-incorporated alginate hydrogels (pMOF@Alg) that selectively adsorbed lithium from aqueous solutions. Results showed that the growth of phosphonate MOF in Cu^{2+}-based alginate hydrogel enhances Li^+ adsorption. Moreover, the carboxylic acid and phosphonate functional groups present in brown algae enhance the lithium adsorption [30]. In 2019, Rudd et al, synthesized a stable luminescent metal-organic framework (LMOF-321) that exhibits a lithium ion-dependent fluorescence intensity at an exceptionally low detection level of 3.3 ppb. This LMOF-321 material demonstrates a high degree of selectivity for Li^+ ions over other light metals. Furthermore, LMOF-321 has a maximum uptake capacity of 12.18 mg/g. This material is used for detecting and adsorption Li^+ from water [31]. In 2021, Qinyan Wei et al. prepared an adsorbent for Li^+ ion from brine based on mil-121, and the adsorption results showed that in the presence of a high concentration (10,000 ppm Li^+), it has an uptake capacity of less than 1.4 mg/g [32]. Weibai Bian et al., in 2021, prepared waste paper cellulose-based Cu-MOF materials threaded by polystyrene sulfonate (WP@PSS@Cu-MOF) for lithium extraction. It had high adsorption capacity and selectivity for Li^+ ions. By combining the size-sieving effects of Cu-MOF with a particular binding affinity of PSS polymer, introducing of PSS into the Cu-MOF matrix significantly improved the selectivity and adsorption capacity for Li^+ ions. It was found that the adsorbent has an uptake capacity of 9.69 mg/g from 150 ppm Li^+ solution [33].

In this study, bimetallic MnO_2@Co/Zn ZIF, which is more chemically stable than ZIF67 (Co ZIF) and ZIF8 (Zn ZIF), is relatively cheap and simple for synthesize, was used to lithium adsorption from an aqueous solution. Furthermore, the influence of temperature, adsorption duration, and initial concentration on the rate of adsorption was investigated, the adsorption isotherm, adsorption rate, and thermodynamic parameters were

calculated, and the ability to recover the adsorbent after several cycles was evaluated.

2. Experimental Section

2.1. Materials

Cobalt (II) nitrate hexahydrate ($Co(NO_3)_2.6H_2O$), Zinc nitrate hexahydrate ($Zn(NO_3)_2 \cdot 6H_2O$), 2-Methylimidazole ($CH_3C_3H_2N_2H$ or 2-mIM), Potassium Permanganate ($KMnO_4$) and were purchased from Sigma Aldrich. Solvents such as ethanol and methanol were purchased from Merck. DI water was also supplied using the distillation system in the laboratory.

2.2. Preparation of ZIFs.

First, the solutions were prepared by dissolving 8 g of 2-mIM and 7 g of $Co(NO_3)_2.6H_2O$, separately, in 80 ml of a mixture of ethanol and methanol at an equal volume ratio. The cobalt nitrate solution was gradually added to the 2-mIM solution and stirred at room temperature at 500 rpm for 24 hrs. To obtain ZIF-67 nanoparticles, the purple precipitate was centrifuged for 10 min at 10,000 rpm, washed three times with EtOH, and dried at 60°C for 24 hrs (Figure1.a).

The same method was used for ZIF-8 synthesis by dissolving 5 g of 2-mIM and 9 g of $Zn(NO_3)_2 \cdot 6H_2O$, separately, in 80 ml of a similar mixture of ethanol and methanol (Figure 1.b).

For the synthesis of bimetallic ZIFs, 1.485 g (5 mmol) of $Zn(NO_3)_2.6H_2O$ and 1.45 g (5 mmol) of $Co(NO_3)_2.6H_2O$ were mixed with 150 ml of a mixture of ethanol and methanol to uniform solution. Then, 6.6 g (80 mmol) of 2-mIM was dissolved in 150 ml of ethanol and methanol to form a clear solution. Methanol and ethanol had an equal volume ratio in the solutions. As the solution of metal salts was stirred (at 500 rpm and room temperature), the 2-mIM solution was added slowly and stirred for 24hrs. To obtain the Co/Zn ZIF nanoparticles, the precipitate was centrifuged for 10 min at 10,000 rpm, washed three times with distilled water and pure ethanol, and dried for 24 hrs at 60°C to remove the solvent.

To deposit MnO_2 nanoparticles on the ZIF surface, 0.5 g of Co/Zn ZIF was dispersed in 100 ml of DI water by sonication for 10 min (solution A). Then, in the ice bath, 100 ml of $KMnO_4$ solution (containing 0.1 g) was introduced into Solution A dropwise with vigorous stirring. After 1 hr, the brown precipitate was collected by centrifugation (15 min and 10000 rpm) and washed three times with DI water. The solution should not have a purple color after washing. The precipitate was dried for 24 hr at 60°C (Figure 2).

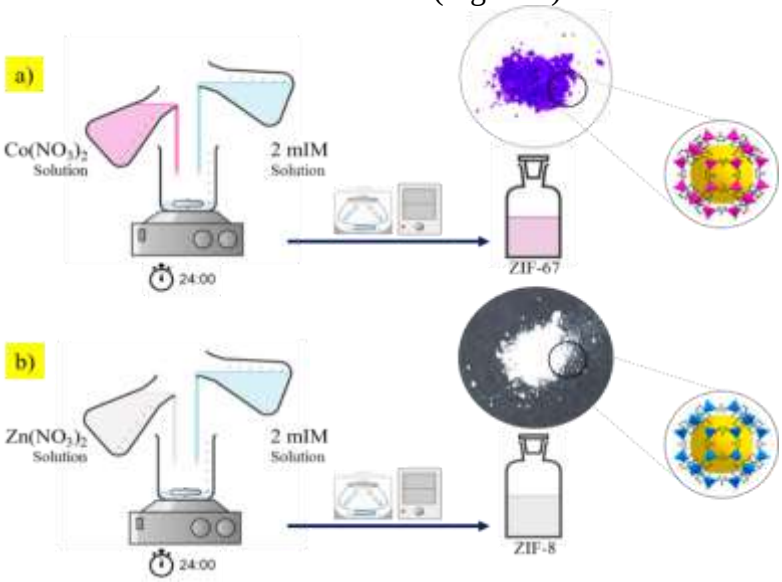

Figure1. *Schematic illustration of a) ZIF-67 and b) ZIF-8 synthesis.*

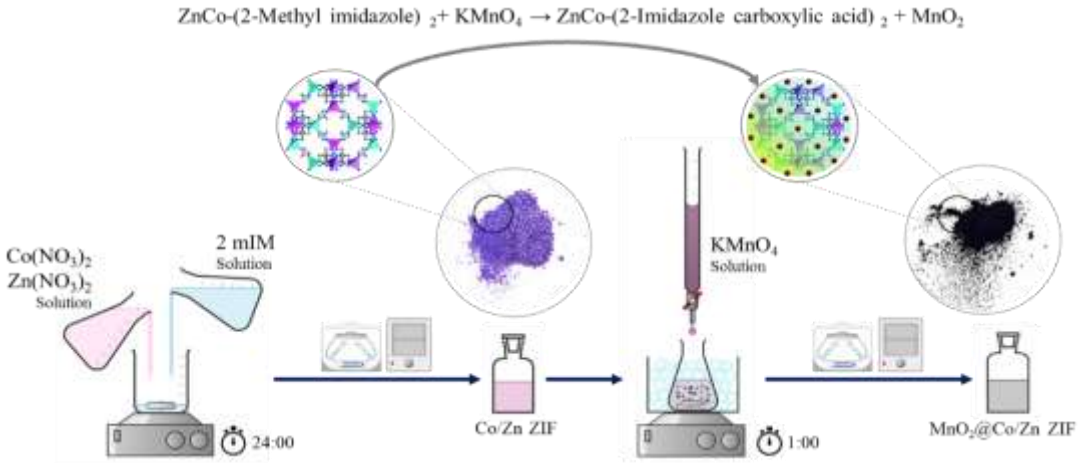

Figure2. *Schematic illustration of MnO_2@Co/Zn ZIF synthesis.*

2.3. Characterizations

X-ray powder diffraction patterns (XRD; STOE STADI MP from Germany) were used to confirm phase purity. The morphology of the synthesized ZIFs was examined using a scanning electron microscope (SEM; ZEISS EVO 18). Li^+ concentrations were measured by inductively coupled plasma mass spectrometry (ICP-MS; Optima 7300 DV ICP-OES). Thermal gravimetric analysis (TGA; Pyris Diamond-Perkin Elmer) was used to determine thermal stability. Pore volume, size, and surface area were calculated using Brunauer-Emmett-Teller (BET; NOVA Station: A Quantachrome). The Bruker ALPHA II spectrometer was used for Fourier transform infrared spectroscopy (FTIR).

2.4. Adsorption properties analysis

The synthesized adsorbents (100 mg) were added to 100 ml of lithium solution with different concentrations (15 to 350 ppm). In a closed container, the solution was stirred at 200 rpm at room temperature and the pH was set at 8-8.5 (the average pH of the ocean). The adsorption time was 24 hrs, and samples were taken at specific intervals. Li^+ concentration was measured by ICP-OES, and the adsorption capacity of Li^+ was calculated by Eq (1).

$$q_e = \frac{(C_0 - C_e) \times V}{m} \qquad (1)$$

In this equation, C_0 and C_e are the initial and final Li^+ concentrations (mg/L), respectively, V is the volume of solution (L), and m represents the mass of the adsorbent (g).

3. Results and discussion

3.1. Characterization.

According to the SEM images and size distribution of the nanostructures shown in Figure 3, the average size of MnO_2@Co/Zn ZIF nanoparticles (164 nm) is larger than Co/Zn ZIF nanoparticles (132 nm). This difference can be attributed to the MnO_2 nanoparticles on the surface of the nanoparticles (MnO_2 nanoparticles on MnO_2@Co/Zn ZIF are shown as white arrows in Figure 3.b).

As shown in Figure 4, N_2 adsorption-desorption profiles of Co/Zn ZIFs and MnO_2@Co/Zn ZIFs revealed BET specific surface areas are 1151.43 and 1049.42 $m^2.g^{-1}$, respectively.

EDX analysis confirms the presence of Cobalt, Zinc, and Manganese metals in the structure of ZIFs, and the element mapping showed that Manganese is uniformly distributed in the ZIFs (Figure 5).

The stability of ZIFs in operational conditions is a crucial parameter in their selection and application. XRD was used to evaluate the stability of the ZIF samples. XRD patterns for synthesized ZIFs are shown in Figure 6. Results proved that

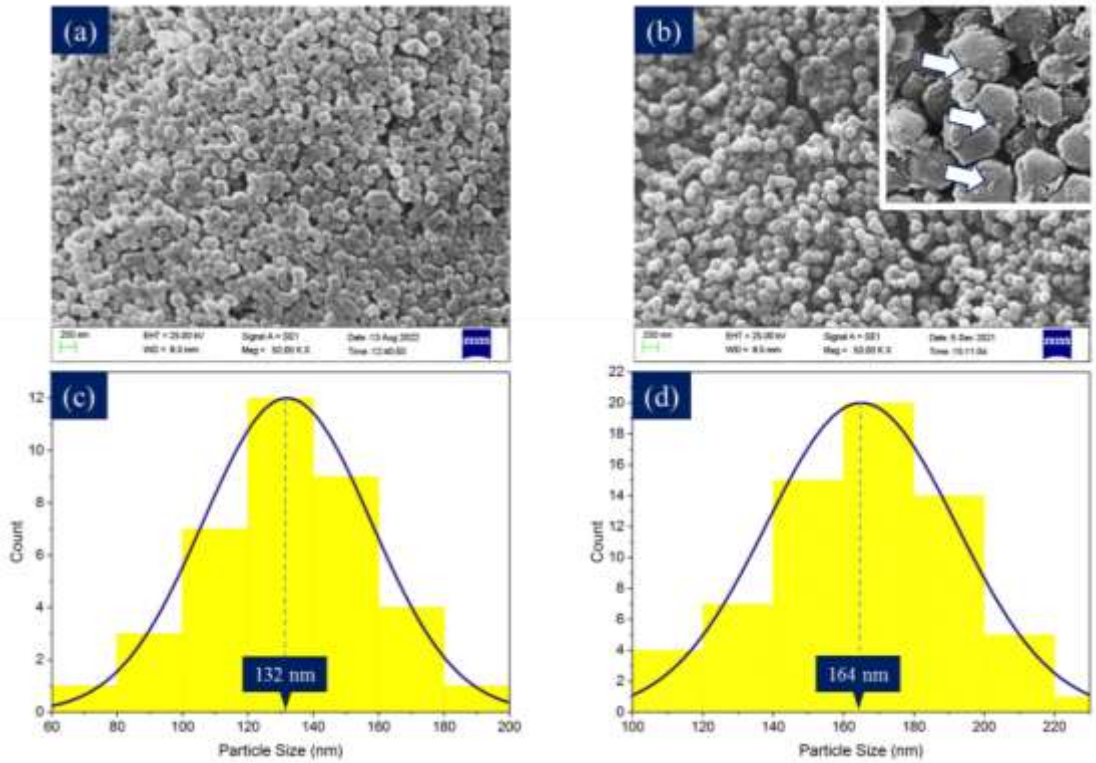

Figure 3. *SEM image of a) Co/Zn ZIF, b) MnO_2@Co/Zn ZIF crystals and their Size Distribution (c, d).*

ZIF67 decomposed in water for a long time. Also, the results showed that at different temperatures and in air or water, ZIF8 and Co/Zn ZIF retain their crystal structures. As shown in Figure 6, the intensity of some peaks in the XRD pattern of MnO_2@Co/Zn ZIFs, indicated by the ● symbol, is lower than that of Co/Zn ZIFs. It can be related to the partial amorphization caused by the presence of $KMnO_4$ solution (as oxidant). Several other peaks, indicated by the ▼ symbol, have increased in intensity, which can be explained by the presence of MnO_2 nanoparticles.

TGA analysis is used to evaluate the thermal stability of the material (Figure 7). The results showed that ZIF67 decomposes at a lower temperature (about 93°C) compared to other nanostructures, whereas the decomposition of other nanostructures occurs at temperatures over 300°C. Due to the presence of inorganic compounds (MnO_2) on the surface of MnO_2@Co/Zn ZIF, the final residual mass value of MnO_2@Co/Zn ZIF is slightly higher than Co/Zn ZIF.

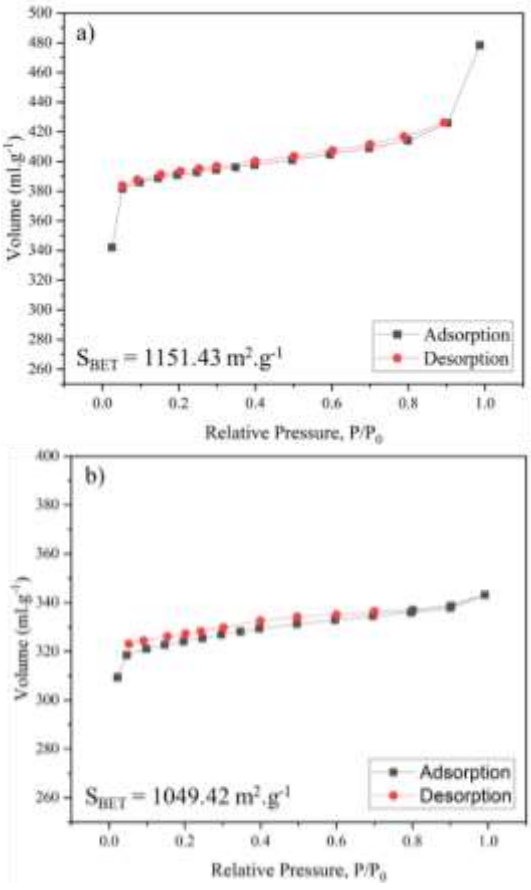

Figure 4. *N_2 adsorption-desorption isotherms of a) Co/Zn ZIF and b) MnO_2@Co/Zn ZIF crystals.*

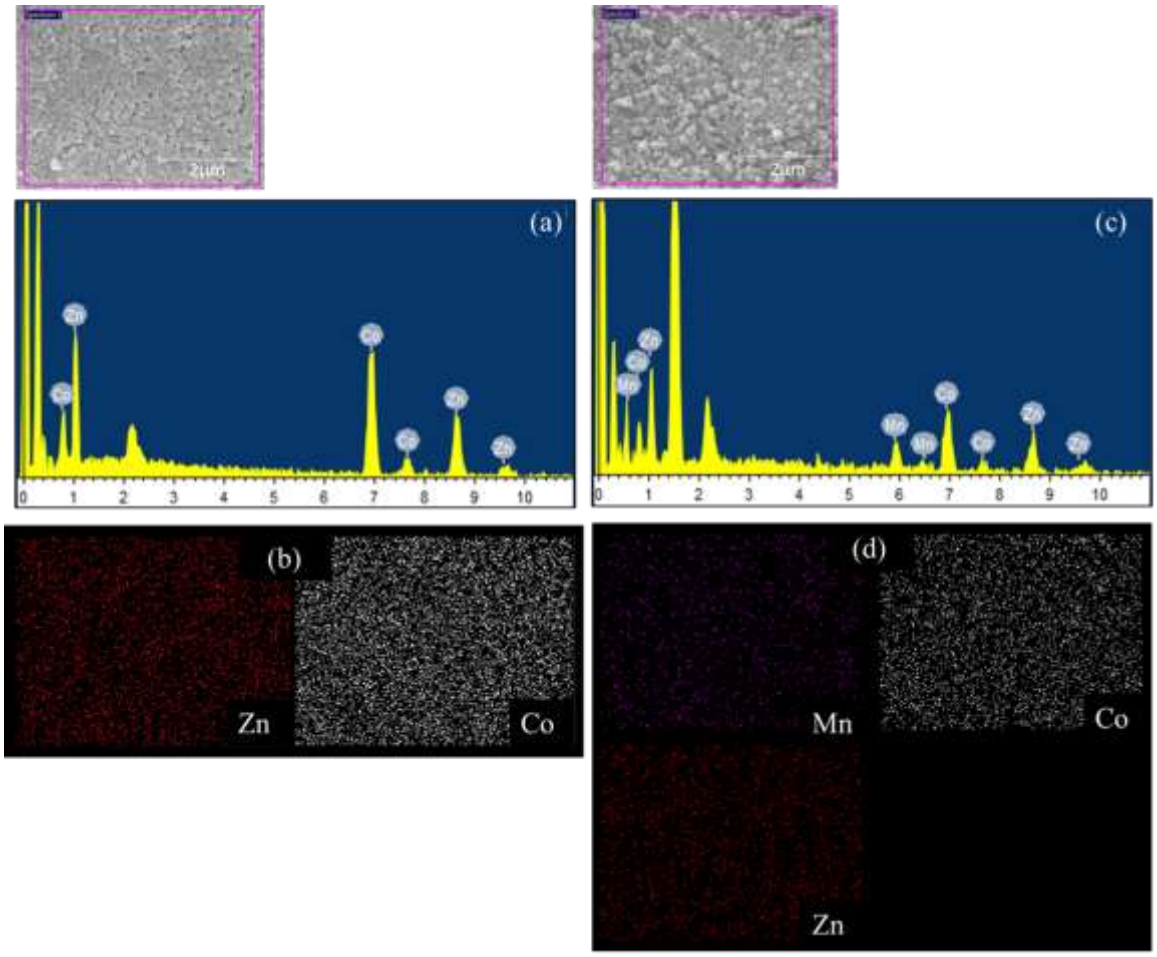

Figure 5. *EDX spectra of a)Co/Zn ZIF, c) MnO_2@Co/Zn ZIF crystals and Co, Zn and Mn element mapping (b, d).*

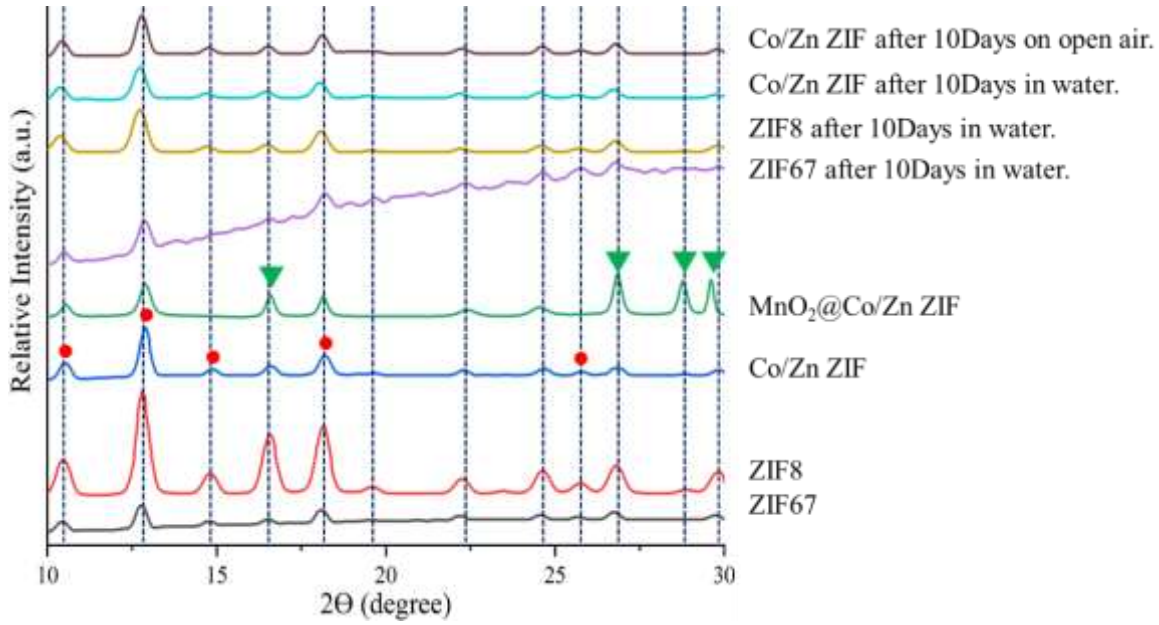

Figure 6. *XRD patterns for ZIFs after various conditions.*

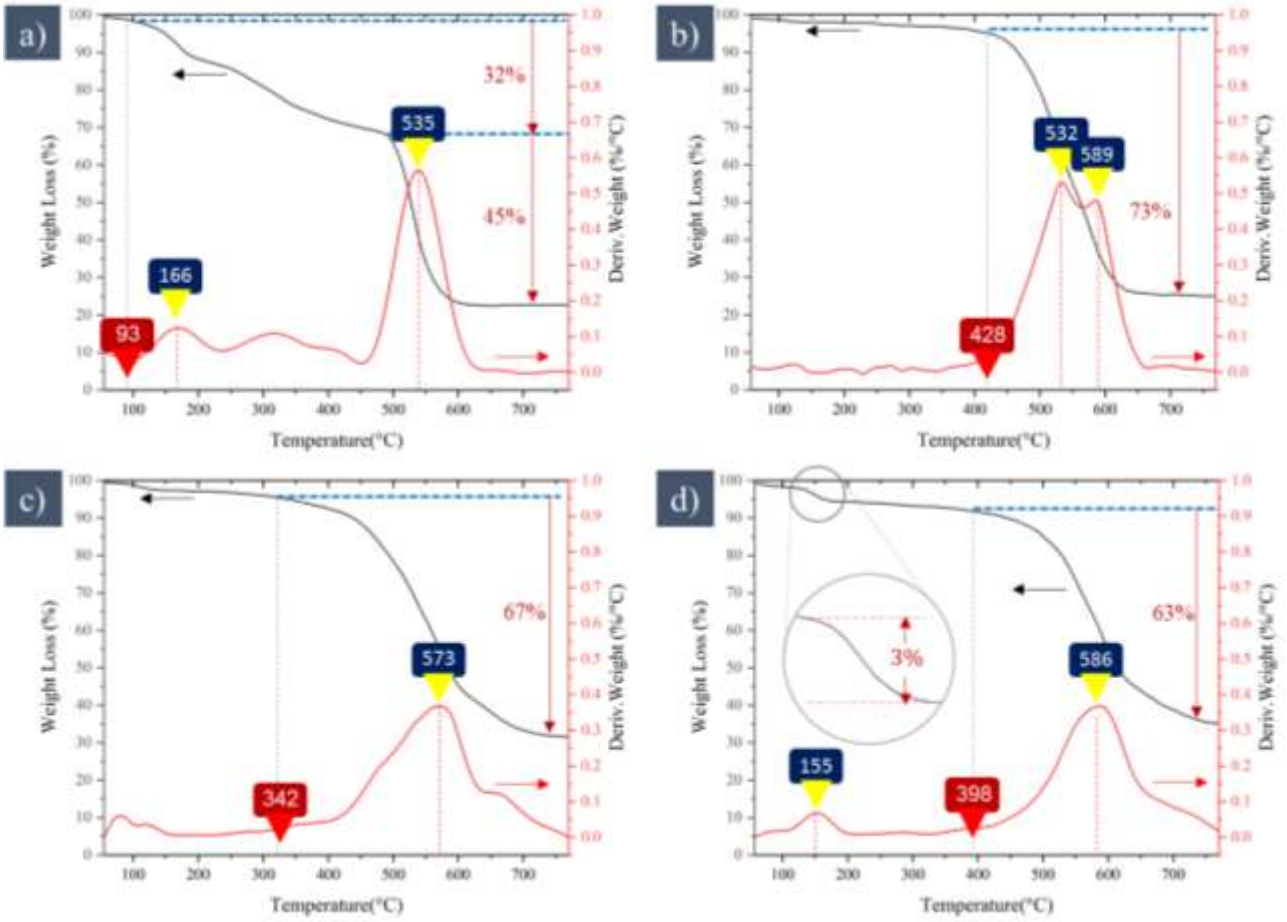

Figure 7. *TGA curves of a) ZIF67, b) ZIF8, c) Co/Zn ZIF, and d) MnO_2@Co/Zn ZIF.*

In MnO_2@Co/Zn ZIF, the gradual weight loss (~3%) from 100 to 200°C was due to the thermal volatilization of surface adsorption and interlayer water (Figure7,d).

FTIR was used to study the coordination of organic ligands (2-mIM) with metals. According to Figure 8, the Spectra of 2-mIM showed a broad band between 3250 and 2250 cm^{-1}, associated with a hydrogen bond between two ligands and a stretching vibration at 1847 cm^{-1}. After coordination with metal ions, these bands entirely disappear from synthesized ZIF materials, indicating deprotonation of the N-H groups of the 2-mIM ligands. Therefore, FTIR confirmed the coordination between metal clusters and organic linkers. The peak at 1575 cm^{-1} corresponds to C=N stretching, while bands between 1350-1500 cm^{-1} can be attributed to ring stretching. The conversion of methyl groups in Co/Zn ZIF to carboxylic groups can be observed by FTIR spectra. A peak at 1632 cm^{-1} can be attributed to carboxylic groups in MnO_2@Co/Zn ZIF. A broad band at 3453 cm^{-1} indicates stretching vibrations between O-H, which demonstrates the hydrated nature of MnO_2 on the surface and interlayer water, which was also mentioned in the discussion of TGA results.

3.2. Adsorption study

The results presented in Figure 9.a demonstrate that the MnO_2@Co/Zn ZIF composite material has a significantly higher lithium adsorption capacity compared to both the ZIF-67 and Co/Zn ZIF materials. This suggests that the MnO_2 nanoparticles incorporated into the composite act as active sites, effectively promoting and enhancing the lithium adsorption capabilities of the material. Figure 9.b shows the amount of Li^+ adsorption at different concentrations and temperatures. As Li^+ concentration incr-easees, adsorption increases. This can be attributed to the following factors: The higher concentration of Li^+ ions in the solution creates a greater driving force between the solid and solution phases. This

increased driving force promotes the transfer of Li^+ ions from the solution to the solid adsorbent, resulting in enhanced adsorption. With a higher concentration of Li^+ ions in the solution, there are more opportunities for these positively charged ions to interact with the active sites or functional groups on the solid adsorbent. This increased ionic interaction between the Li^+ ions and the adsorbent surface further enhances the adsorption process. According to the adsorption data, the lithium adsorption capacity by MnO_2@Co/Zn ZIF increases with temperature, indicating that the adsorption process is endothermic in nature.

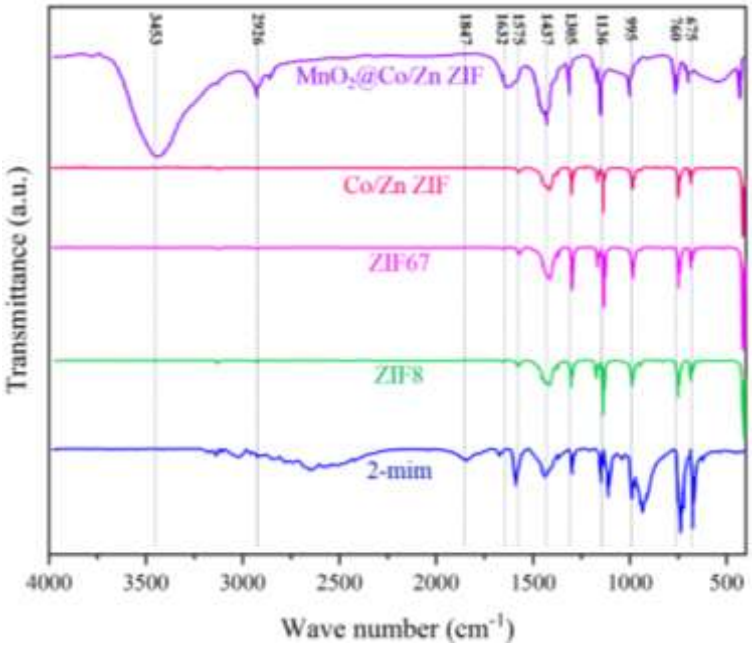

Figure 8. *FTIR spectra of ZIF series compared with 2-methylimidazole (2-mIM).*

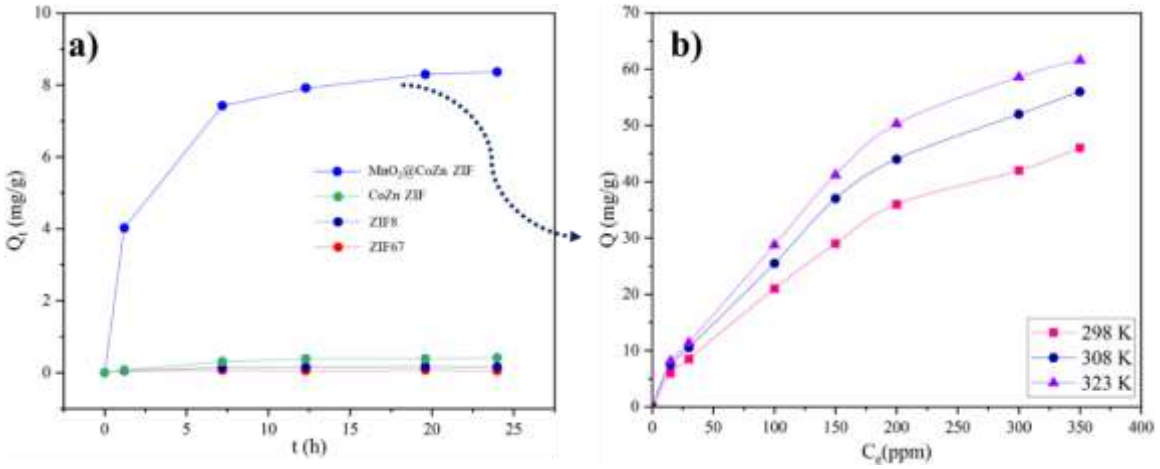

Figure 9. *a) Comparison of lithium adsorption by ZIF67, Co/Zn ZIF and MnO_2@Co/Zn ZIF adsorbents. (t=24 hrs, $C_0(Li^+)$=38 ppm , m(adsorbent)=100 mg , V=100 ml , T=298K , pH=8.5) and b) Adsorption isotherms of MnO_2@Co/Zn ZIF (t=24 hrs, $C_0(Li^+)$=15-350 ppm , m(adsorbent)=100 mg , V=100 ml , T=298K , pH=8.5)*

Adsorption isotherm models are essential designing adsorption systems since they describe the adsorption progress and present the adsorption mechanism. Adsorption equilibrium data provide information about how much adsorbent is required per unit of adsorbed. Here, Langmuir and Freundlich models were examined for experimental data.

The Langmuir adsorption isotherm, which assumes adsorption occurs at homogeneous sites on the adsorbent, can model a wide variety of adsorption processes. The equation describing the linearized Langmuir isotherm (Eq2)[34]:

$$\frac{C_e}{q_e} = \frac{1}{K_L q_m} + \frac{C_e}{q_m} \qquad (2)$$

where C_e is the equilibrium concentration of Li^+ (mg/L), q_e is the equilibrium adsorption capacity in mg/g, K_L is the Langmuir adsorption constant (L/mg), and q_m is the maximum adsorption capacity in mg/g. Figure 10.a shows the correlation of lithium adsorption data by MnO_2@Co/Zn ZIF with the Langmuir isotherm.

In the Freundlich isotherm model, the adsorption surface is heterogeneous with different adsorption energies and does not provide information about monolayer adsorption. This model can be expressed as a linear equation (Eq3) [35]:

$$\log q_e = \log K_F + \frac{1}{n} \log C_e \qquad (3)$$

K_F is a constant related to the adsorption affinity, and n is the heterogeneity coefficient. Figure 10.b shows the fitting of adsorption data in the Freundlich isotherm.

According to Figure 10, at T=298K and lower concentrations (<200ppm), it is better fitted by Freundlich isotherm (R^2=0.995) than Langmuir isotherm (R^2=0.901), which can be attributed to that the adsorption at lower concentrations is heterogeneous since the MnO_2 on the surface and Co/Zn ZIF structure has not yet saturated with lithium (Figure 11-a). At higher concentrations (>200 ppm), Langmuir isotherm (R^2=0.987) shows a better fit than Freundlich isotherm (R^2=0.979), showing that adsorption occurs homogeneously and only on the Co/Zn ZIF surface at high concentrations when the more active adsorption sites (MnO_2 nanoparticles) are saturated with lithium (Figure 11-b). It also happens at other temperatures.

For lithium adsorption from low-concentration water resources (such as seawater), the Freundlich isotherm, which is more fit at low concentrations, is considered the main adsorption isotherm. The parameters of Langmuir and Freundlich isotherms obtained from fitting the adsorption data at different temperatures are given in Table 1.

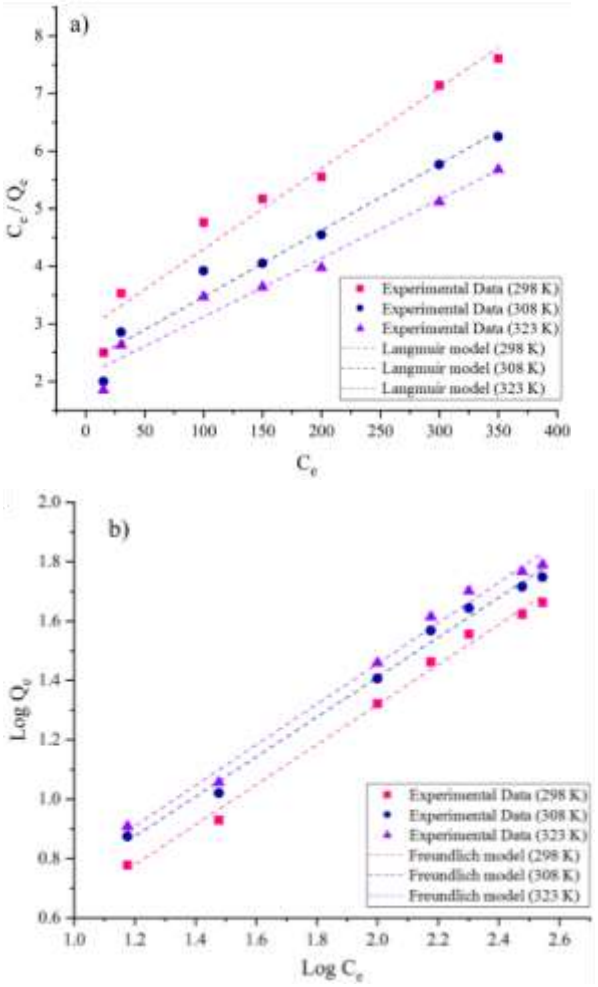

Figure10. *Adsorption isotherms of MnO_2@Co/Zn ZIF a) Langmuir and b) Freundlich models.*

As shown in Table 1, The Freundlich isotherm fits the adsorption data with a higher correlation coefficient, indicating a heterogeneous adsorption surface [36].

According to the n value in Freundlich isotherm, linear adsorption occurs if n = 1, chemisorption occurs at n<1, and physisorption at n >1. Based on the value of n in table1, the adsorption of Li^+ ions followed a multilayer physical adsorption

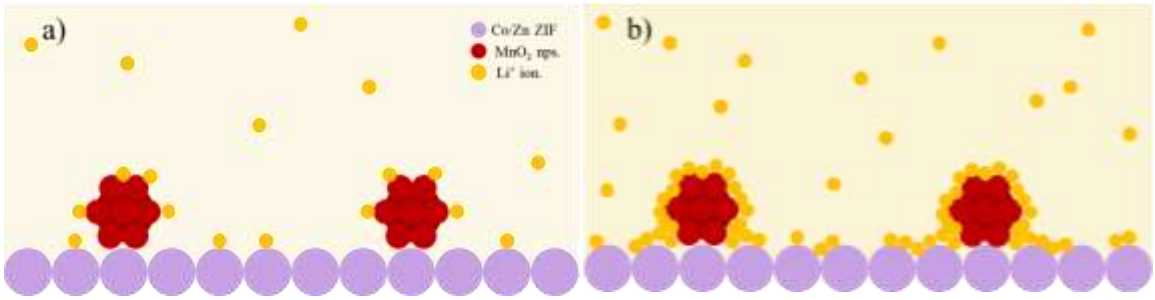

Figure 11. *Schematic of lithium adsorption with MnO_2@Co/Zn ZIF at a) low and b) high concentrations.*

Table 1. *Langmuir and Freundlich isotherm parameters.*

T(K)	Freundlich			Langmuir		
	K_F	n	R^2	Q_m	K_L	R^2
298	0.931	1.482	0.994	71.43	0.00483	0.964
308	1.172	1.490	0.993	86.96	0.00495	0.963
323	1.229	1.463	0.991	98.04	0.00485	0.965

mechanism [36]. n represents the intensity of sorption or the heterogeneity of the surface. Based on Table 1, the value of n at 323 K has decreased compared to lower temperatures, indicating an increase in the homogeneity of the adsorption surface. Experimental data were obtained at three different temperatures to calculate the thermodynamic parameters of lithium adsorption with MnO_2@Co/Zn ZIF at various temperatures (298 K, 308 K, and 323 K). The following equations were used to calculate the thermodynamic parameters: standard enthalpy (ΔH°), standard entropy (ΔS°), and standard Gibbs free energy (ΔG°) changes (Eq 4-6) [37]:

$$\Delta G^{\circ} = \Delta H^{\circ} - T\Delta S^{\circ} \quad (4)$$

$$\Delta G^{\circ} = -RT \ln K_d \quad (5)$$

$$\ln K_d = \frac{\Delta S^{\circ}}{R} - \frac{\Delta H^{\circ}}{RT} \quad (6)$$

K_d is the adsorption distribution coefficient, T is the absolute temperature, and R is the gas constant. By analyzing the dimensions of K_d and K_F of the Freundlich isotherm model with C_e and q_e in $mg.L^{-1}$ and $mg.g^{-1}$, the following equation can be developed (Eq 7,8)[37]:

$$K_{eq} = K_F M_w(T)\left(\frac{1}{\frac{M_W(T)}{1000}}\right)^{\left(1-\frac{1}{n}\right)} \quad (7)$$

$$K_d = K_{eq} \quad (8)$$

where M_w (T) is the mass of water per liter ($g\ L^{-1}$) at a temperature T, K_{eq} and K_F are the equilibrium and Freundlich isotherm constant, respectively.

Based on equation 5, ΔG was calculated at different temperatures. ΔS and ΔH were determined by plotting ΔG versus temperature according to equation 4 (Figure 12). Thermodynamic parameters for lithium adsorption are given in Table 2.

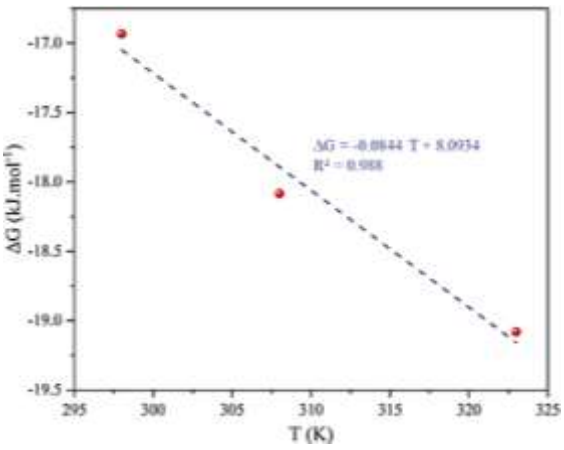

Figure 12. *ΔG plot in terms of T(K) to calculate the value of ΔS and ΔH according to (Eq4).*

ΔG values were negative at all temperatures, indicating spontaneous and

thermodynamically favorable lithium adsorption by MnO_2@Co/Zn ZIF. The ΔG value decreases with increasing temperature, indicating that the driving force for lithium adsorption becomes stronger. Additionally, it shows that lithium adsorbs more spontaneously at higher temperatures. The positive values of ΔH demonstrated that the lithium adsorption processes were endothermic. The heat of adsorption of 80 kJ/mol or more indicates chemisorption and lower values indicate physisorption [38]. So, based on the value of ΔH (8.094 kJ/mol), lithium adsorption can be attributed to physisorption. The positive value of entropy (ΔS°) proposes an increased randomness at the surface-solution interface during lithium adsorption. The displacement of H^+ increases the randomness of the system as it gains more translation entropy than Li^+ loses during lithium adsorption.

Table 2. *Thermodynamic parameters from isotherm constant.*

T (K)	K_{eq}	ΔG (kJ.mol^{-1})	ΔH (kJ.mol^{-1})	ΔS (J.mol^{-1}.K^{-1})
298	929.5	-16.933		
308	1167.2	-18.085	8.094	84.4
323	1218.5	-19.081		

A study of the adsorption kinetics of lithium in aqueous solutions, such as brine and seawater, is essential for optimizing the extraction process. The pseudo-first-order and pseudo-second-order model can be expressed as (Eq 9, 10) [39, 40]:

$$\ln(q_e - q_t) = \ln q_e - \mathrm{K}_1 t \qquad (9)$$

$$\frac{t}{q_t} = \frac{1}{K_2 q_e^2} + \frac{1}{q_e} t \qquad (10)$$

According to Figure 13, the pseudo-second-order kinetic model provided a better fit to the experimental data for lithium adsorption using MnO_2@Co/Zn ZIF adsorbent compared to the pseudo-first-order model, as evidenced by the higher correlation coefficient (R^2) value. Table 3 shows the parameters of the kinetic models and the correlation coefficient. Pseudo-second-order kinetics demonstrated that adsorbate and adsorbent concentrations in the adsorption process are involved in determining the rate, which could be a chemical sorption process.

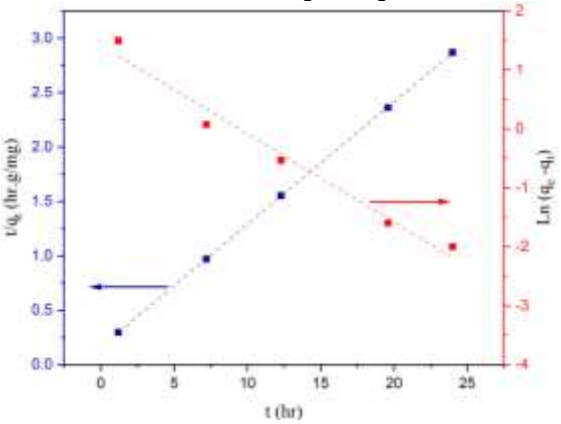

Figure 13. *Kinetic models: pseudo-first-order (Ln(qe-qt) vs t) and (b) pseudo-second-order (t/qt vs t).*

3.3. Desorption Performance

The desorption process was carried out for the adsorbed lithium ions at initial concentrations of 30, 150, and 350 ppm. For this purpose, 0.1 g of lithium-saturated adsorbent was immersed in 500 ml of 0.2 M HCl solution and stirred (at 500 rpm) for 6 hrs at room temperature. The desorption percentages (D(%)) were determined by Eq. (11), and desorption data are given in Figure 14.a.

$$D(\%) = \frac{R}{S} \times 100 \qquad (11)$$

S indicates the amount of Li^+ previously adsorbed, and R represents the amount of Li^+ that was recovered. It is proposed that desorption occurs when Li^+ ions replace H^+ ions at the surface of an adsorbent in an eluting media (HCl). This study showed that MnO_2@Co/Zn ZIF has a great desorption ability and is a good candidate for the recovery of large amounts of Li^+.

Several adsorption-regeneration experiments were conducted in order to evaluate the possibility of recycling the adsorbent for reuse in multiple adsorption cycles. Lithium-loaded MnO_2@Co/Zn ZIF was regenerated by adding it to 0.2 M HCl solution and stirring at 25°C for 6 hours.

The MnO_2@Co/Zn ZIF was regenerated after complete desorption by continuously washing with deionized water until a neutral pH was reached, followed by drying at 60°C. Adsorption-regeneration cycles were repeated three times, and the lithium sorption capacity was measured after each cycle. The lithium adsorption capacity decreased slightly after each regeneration cycle.

Table 3. *First- and second-order kinetics parameters.*

q_e (mg/g)	Pseudo-First-order			Pseudo-second-order		
	k_1 (h^{-1})	q_e(mg/g)	R^2	k_2 (h.g/mg)	q_e(mg/g)	R^2
8.50	0.15	4.12	0.98	0.24	6.13	0.99

After the first cycle, the adsorption capacity was 97.6% of the original capacity. This dropped to 91.5% after the second cycle and 87.4% after the third cycle, as shown in Figure 14.b. The reduction in the amount of adsorption may be due to the desorption process not being fully completed.

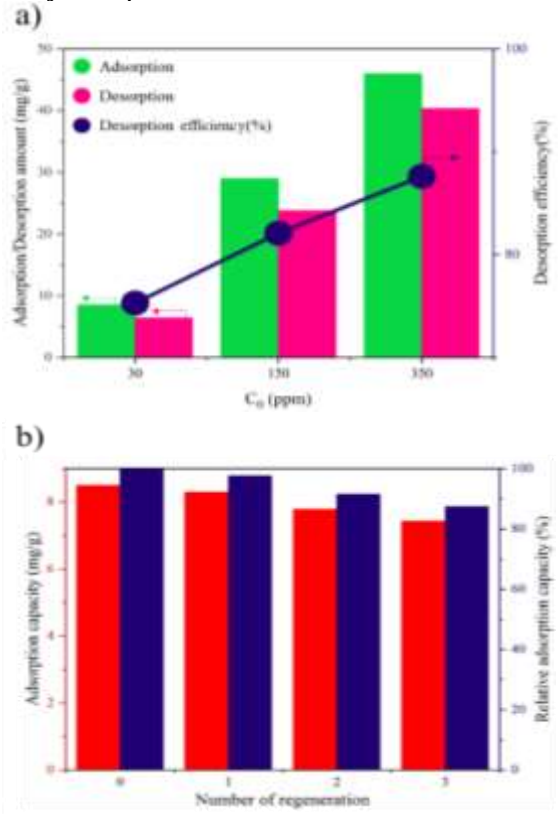

Figure 14. *a) Desorption efficiency of Li^+ vs Li^+ initial concentrations and b) Regeneration efficiency of MnO_2@Co/Zn ZIFs.*

4. CONCLUSION

In this research, metal-organic framework (MOF) materials were employed as adsorbents to selectively remove and recover lithium ions from solutions. MnO_2 nanoparticles were deposited on the surface of Co/Zn ZIFs to enhance selective lithium adsorption. BET analysis proved that the inserting of MnO_2 nanoparticles on the Co/Zn ZIF surface does not

ACKNOWLEDGEMENT

The authors would like to express their sincere appreciation to Dr. Mehdi Akbari, Dr. Saba Raveshian, and Dr. Mahdieh Yavari for their valuable contributions to this work.

CONFLICT OF INTEREST

The authors declare that they have no conflict of interest.

REFERENCES

1. Kavanagh, L., "Global lithium sources—industrial use and future in the electric vehicle industry: a review", *Resources*, 7(3) (2018) 57.
2. Yang, S., "Lithium metal extraction from seawater", *Joule*, 2(9) (2018) 1648-1651.
3. Rashed, M. N., *Adsorption technique for the removal of organic pollutants from water and wastewater*. Organic pollutants-monitoring, risk and treatment, 2013. 7: p. 167-194.
4. Weng, D., "Introduction of manganese based lithium-ion Sieve-A review*"*, *Progress in Natural Science Materials International*, 30(2) (2020) 139-152.

5. Butt, F. S., "Lithium harvesting from the most abundant primary and secondary sources: A comparative study on conventional and membrane technologies", *Membranes*, 12(4) (2022) 373.
6. Ding, T., "Polyacrylonitrile/Crown Ether Composite Nanofibres With High Efficiency for Adsorbing Li (I): Experiments and Theoretical Calculations*", Frontiers in Energy Research*, (2021) 828.
7. Yuan, C., "Highly selective lithium ion adsorbents: polymeric porous microsphere with crown ether groups", *Transactions of Tianjin University*, 25 (2019) 101-109.
8. Díez, E., "Zeolite Adsorbents for Selective Removal of Co (II) and Li (I) from Aqueous Solutions", *Water*, 15(2) (2023) 270.
9. Kamran, U., "Chemically modified activated carbon decorated with MnO2 nanocomposites for improving lithium adsorption and recovery from aqueous media", *Journal of Alloys and Compounds*, 794 (2019) 425-434.
10. Al-Absi, R. S., "Novel composite materials of modified roasted date pits using ferrocyanides for the recovery of lithium ions from seawater reverse osmosis brine", *Scientific Reports*, 11(1) (2021) 18896.
11. Yu, S., "Recent advances in metal-organic framework membranes for water treatment: A review", *Science of the Total Environment*, 800 (2021) 149662.
12. Safaei, M., "A review on metal-organic frameworks: Synthesis and applications", *TrAC Trends in Analytical Chemistry*, 118 (2019) 401-425.
13. Nasihat Sheno, N., Morsali, A., "Synthesis of Different Copper Oxide Nano-Structures From Direct Thermal Decomposition of Porous Copper (II) Metal-Organic Framework Precursors", *International Journal of Nanoscience and Nanotechnology*, 8(2) (2012) 99-104.
14. Safari, M., "Magnetic metal-organic frameworks for the extraction of trace amounts of heavy metal ions prior to their determination by ICP-AES", *Microchimica Acta*, 184(5) (2017) 1555-1564.
15. Sohrabi, M. R., "Solid phase extraction of Cd (II) and Pb (II) using a magnetic metal-organic framework, and their determination by FAAS", *Microchimica Acta*, 180(7) (2013) 589-597.
16. Liu, W., "Highly sensitive and selective uranium detection in natural water systems using a luminescent mesoporous metal–organic framework equipped with abundant Lewis basic sites: a combined batch, X-ray absorption spectroscopy, and first principles simulation investigation", *Environmental science & technology*, 51(7) (2017) 3911-3921.
17. Tahmasebi, E., "Application of mechanosynthesized azine-decorated zinc (II) metal–organic frameworks for highly efficient removal and extraction of some heavy-metal ions from aqueous samples: a comparative study", *Inorganic chemistry*, 54(2) (2015) 425-433.
18. Taghizadeh, M., "A novel magnetic metal organic framework nanocomposite for extraction and preconcentration of heavy metal ions, and its optimization via experimental design methodology", *Microchimica Acta*, 180(11) (2013) 1073-1084.
19. Jamali, A., "Lanthanide metal–organic frameworks as selective microporous materials for adsorption of heavy metal ions", *Dalton Transactions*, 45(22) (2016) 9193-9200.
20. Salarian, M., "A metal-organic framework sustained by a nanosized Ag12 cuboctahedral node for solid-phase extraction of ultra traces of lead (II) ions", *Microchimica Acta*, 181(9) (2014) 999-1007.
21. Wang, Y., "Preparation of magnetic metal organic frameworks adsorbent modified with mercapto groups for the extraction and analysis of lead in food samples by flame atomic absorption spectrometry", *Food Chemistry*, 181 (2015) 191-197.
22. Wang, Y., "A magnetic metal-organic framework as a new sorbent for solid-phase extraction of copper (II), and its determination by electrothermal AAS", *Microchimica Acta*, 181(9) (2014) 949-956.
23. Bagheri, A., "Synthesis and characterization of magnetic metal-organic framework (MOF) as a novel sorbent, and its optimization by experimental design methodology for determination of palladium in environmental samples", *Talanta*, 99 (2012) 132-139.
24. Wang, Y., "Preparation of a functionalized magnetic metal–organic framework sorbent for the extraction of lead prior to electrothermal atomic absorption spectrometer analysis", *Journal of Materials Chemistry A*, 1(31) (2013) 8782-8789.
25. Tokalıoğlu, Ş., "Zirconium-based highly porous metal-organic framework (MOF-545) as an efficient adsorbent for vortex assisted-solid phase extraction of lead from cereal, beverage and water samples", *Food chemistry*, 237 (2017) 707-715.
26. Moghaddam, Z. S., "Synthesis of UiO-66-OH zirconium metal-organic framework and its application for selective extraction and trace determination of thorium in water samples by spectrophotometry", *Spectrochimica Acta Part A: Molecular and Biomolecular Spectroscopy*, 194 (2018) 76-82.
27. Liu, W., "Ratiometric monitoring of thorium contamination in natural water using a dual-emission luminescent europium organic framework", *Environmental science & technology*, 53(1) (2018) 332-341.
28. Sohrabi, M. R., "Preconcentration of mercury (II) using a thiol-functionalized metal-organic framework nanocomposite as a sorbent", *Microchimica Acta*, 181(3) (2014) 435-444.

29. Zhang, H., “Ultrafast selective transport of alkali metal ions in metal organic frameworks with subnanometer pores”, *Science advances*, 4(2) (2018) eaaq0066.
30. Park, S. H., “Selective lithium and magnesium adsorption by phosphonate metal-organic framework-incorporated alginate hydrogel inspired from lithium adsorption characteristics of brown algae”, *Separation and Purification Technology*, 212 (2019) 611-618.
31. Rudd, N. D., “Luminescent Metal–Organic Framework for Lithium Harvesting Applications”, *ACS Sustainable Chemistry & Engineering*, 7(7) (2019) 6561-6568.
32. Wei, Q., “Simple and Rapid Preparation of MIL-121 with Small Particles for Lithium Adsorption from Brine”, *Coatings*, 11(7) (2021) 854.
33. Bian, W., “A novel waste paper cellulose-based Cu-MOF hybrid material threaded by PSS for lithium extraction with high adsorption capacity and selectivity”, *Cellulose*, 28(5) (2021) 3041-3054.
34. Langmuir, I., “The adsorption of gases on plane surfaces of glass, mica and platinum”, *Journal of the American Chemical society*, 40(9) (1918) 1361-1403.
35. Freundlich, H., “Over the adsorption in solution”, *J. Phys. chem*, 57(385471) (1906) 1100-1107.
36. Ryu, T., “Recovery of lithium ions from seawater using a continuous flow adsorption column packed with granulated chitosan–lithium manganese oxide”, *Industrial & Engineering Chemistry Research*, 55(26) (2016) 7218-7225.
37. Ghosal, P. S., Gupta, A. K., “An insight into thermodynamics of adsorptive removal of fluoride by calcined Ca–Al–(NO 3) layered double hydroxide”, *RSC advances*, 5(128) (2015) 105889-105900.
38. Abdulsalam, J., “Equilibria and isosteric heat of adsorption of methane on activated carbons derived from South African coal discards”, *ACS omega*, 5(50) (2020) 32530-32539.
39. Lagergren, S. K., “About the theory of so-called adsorption of soluble substances”, *Sven. Vetenskapsakad. Handingarl*, 24 (1898) 1-39.
40. Ho, Y.-S., McKay, G., “Pseudo-second order model for sorption processes”, *Process biochemistry*, 34(5) (1999) 451-465.